



**Extension of a gaseous dry deposition algorithm to oxidized volatile organic compounds
and hydrogen cyanide for application in chemistry transport models**

Zhiyong Wu^{1,2}, Leiming Zhang^{1,*}, John T. Walker³, Paul A. Makar¹, Judith A. Perlinger⁴,
Xuemei Wang⁵

¹Air Quality Research Division, Science and Technology Branch, Environment and Climate
Change Canada, Toronto, ON, M3H 5T4, Canada

²ORISE Fellow at US Environmental Protection Agency, National Risk Management Research
Laboratory, Research Triangle Park, NC, 27711, USA

³US Environmental Protection Agency, National Risk Management Research Laboratory,
Research Triangle Park, NC, 27711, USA

⁴Civil & Environmental Engineering Department, Michigan Technological University,
Houghton, MI, 49931, USA

⁵Institute for Environmental and Climate Research, Jinan University, Guangzhou, 510632, China

*Correspondence to: Leiming Zhang (leiming.zhang@canada.ca)



1 **Abstract:** With increasing complexity of air quality models, additional chemical species have been
2 included in model simulations for which dry deposition processes need to be parameterized. For
3 this purpose, the gaseous dry deposition scheme of Zhang et al. (2003) is extended to include 12
4 oxidized volatile organic compounds (oVOCs) and hydrogen cyanide (HCN) based on their
5 physicochemical properties, namely the effective Henry's law constants and oxidizing capacities.
6 Modeled dry deposition velocity (V_d) values are compared against field flux measurements over a
7 mixed forest in the southeastern U.S. during June 2013. The model captures the basic features of
8 the diel cycles of the observed V_d . Modeled V_d values are comparable to the measurements for
9 most of the oVOCs at night. However, modeled V_d values are mostly around 1 cm s^{-1} during
10 daytime, which is much smaller than the observed daytime maxima of $2\text{-}5 \text{ cm s}^{-1}$. Analysis of the
11 individual resistance terms/uptake pathways suggests that flux divergence due to fast atmospheric
12 chemical reactions near the canopy was likely the main cause of the large model-measurement
13 discrepancies during daytime. The extended dry deposition scheme likely provides conservative
14 V_d values for many oVOCs. While higher V_d values and bi-directional fluxes can be simulated by
15 coupling key atmospheric chemical processes into the dry deposition scheme, we suggest that more
16 experimental evidence of high oVOC V_d values at additional sites is required to confirm the
17 broader applicability of the high values studied here. The underlying processes leading to high
18 measured oVOC V_d values require further investigation.



19 1. Introduction

20 Atmospheric pollutants impact human health and can also cause detrimental effects on sensitive
21 ecosystems (Wright et al., 2018). Quantifying atmospheric deposition for atmospheric pollutants
22 is needed to estimate their lifetimes in air and deposition rates to ecosystems. The amount of dry
23 deposition of a pollutant of interest is typically calculated as the product of its ambient
24 concentration and its dry deposition velocity (V_d), with V_d being calculated using empirically
25 developed dry deposition schemes (Wesely & Hicks, 2000). Existing dry deposition schemes are
26 known to have large uncertainties even for the most commonly studied chemical species such as
27 O_3 , SO_2 and more commonly measured nitrogen species with relatively rich flux datasets (Flechard
28 et al., 2011; Wu et al., 2012; Wu et al., 2018).

29 Existing dry deposition schemes have thus far considered a small number of oxidized
30 volatile organic compounds (oVOCs). Due to the lack of field flux data of oVOCs, V_d of these
31 species is typically parameterized based on physicochemical properties, taking SO_2 and O_3 as
32 references (Wesely, 1989; Zhang et al., 2003). However, Karl et al. (2010) found that V_d of oVOCs
33 calculated using existing schemes are about a factor of 2 lower than those based on canopy-level
34 concentration gradient measurements over six forest and shrubland sites. V_d in their study was
35 calculated from an inverse Lagrangian transport model with concentration gradient data as model
36 input. The ratio of magnitudes between $V_d(\text{oVOCs})$ and $V_d(O_3)$ in the study of Karl et al. (2010)
37 are similar to those of Zhang et al. (2003) in that $V_d(\text{oVOCs})$ is slightly smaller than $V_d(O_3)$ in both
38 cases. However, the typical daytime $V_d(O_3)$ over vegetated canopies is around 1 cm s^{-1} in the
39 literature from numerous studies (see summary in Silva & Heald, 2018), and the value in Karl et
40 al. (2010) is much higher (e.g., up to 2.4 cm s^{-1} at canopy top). One hypothesis explaining both
41 high $V_d(O_3)$ and high $V_d(\text{oVOCs})$ would be the reaction of O_3 with oVOC, which depends on the



42 chemical structure of the oVOC, but data required for validating this hypothesis are still lacking.
43 We thus suspect that the very high $V_d(\text{oVOCs})$ presented in Karl et al. (2010) were likely caused
44 by atmospheric chemical processes not typically considered in the dry deposition process. High
45 $V_d(\text{oVOCs})$ values were also observed over a temperate mixed forest in the southeastern U.S. in a
46 more recent short-term study (Nguyen et al., 2015), which again were suspected to be caused by
47 atmospheric chemical reactions near vegetation surface. The flux measurements themselves also
48 contain uncertainty. For example, Wu et al. (2015) showed that different measurement methods
49 (e.g., flux-gradient versus eddy correlation) resulted in very different daytime $V_d(\text{O}_3)$ over the same
50 forest canopy. Hydrogen cyanide (HCN) is one of the most abundant cyanides present in the
51 atmosphere (Singh et al., 2003) and is considered a biomass burning marker (Bunkan et al., 2013),
52 but few existing studies have considered its dry deposition, which is critical to estimating the total
53 sinks and atmospheric lifetimes of cyanides.

54 To fulfill community demands of modeling dry deposition of organic compounds (Kelly et
55 al., 2019; Moussa et al., 2016; Paulot et al., 2018; Pye et al., 2015; Xie et al., 2013) and to take
56 advantage of the recent flux dataset of a large number of oVOCs and HCN (Nguyen et al., 2015),
57 the present study extends the current Zhang et al. (2003) scheme by including 12 additional oVOC
58 species and HCN. The parameterization for these newly-included species is based on the effective
59 Henry's law constants and oxidizing capacities of the individual species and by considering the
60 measured V_d values as well. Model-measurement comparison is conducted for V_d as well as
61 resistance components/uptake pathways, results from which identify the major causes of model-
62 measurement discrepancies. Model parameters were chosen to produce the magnitude of nighttime
63 V_d for nearly all the chemical species, but this approach inevitably underpredicted daytime V_d
64 values for several oVOCs species with very high measured daytime V_d values. This approach is



65 recommended due to the following considerations: (1) some of the chemical processes causing
66 flux loss at the surfaces may be treated separately in the mass continuity equation in chemical
67 transport models, (2) some of the oVOCs may also experience bi-directional air-surface exchange,
68 and (3) more flux measurements are needed to confirm if the very high daytime flux for certain
69 oVOCs is an universal phenomenon, noting that the existing data used here were from a short
70 period of several days and over only one surface type.

71 At this stage with very limited knowledge on oVOC V_d , air-surface exchange models based
72 on various theoretical and/or measurement approaches should be developed, so that these models
73 can be made available to the scientific community where such models are urgently needed, and for
74 future evaluation and improvement should more flux measurements become available. For
75 example, Nguyen et al. (2015) modified the Wesely (1989) scheme to fit the flux data, while in
76 the present study a more theoretically constrained approach was used. A more sophisticated model
77 for handling air-canopy exchange of semivolatile organic compounds is also available in the
78 literature (Nizzetto and Perlinger, 2012). Note that a bottom-up approach was adopted in Nizzetto
79 and Perlinger (2012) to estimate fluxes as compared to the present study, which provides a top-
80 down determination of deposition velocity through comparison with measured (bottom-up) fluxes.
81 oVOC V_d values from all the existing models may all be within the uncertainty range.

82

83 **2. Methodology**

84 Dry deposition of a gaseous compound to most canopy types is mainly through nonstomatal uptake
85 during nighttime and through both nonstomatal and stomatal uptake during daytime. The
86 nonstomatal uptake depends on water solubility and reactivity of the species, which can be



87 quantified by its effective Henry's Law constant (H^*) and oxidizing capacity, respectively (Wesely,
88 1989; Zhang et al., 2002). In the Supporting Information (SI) document, Table S1 lists H^* values
89 and Table S2 lists the oxidizing capacities for oVOCs and HCN considered in the present study.
90 Following the approach described in Zhang et al. (2002), two model parameters (α and β) are
91 needed for every chemical species to calculate the nonstomatal uptake, with α being dependent on
92 H^* and β dependent on oxidizing capacity. Initial α values were first given based the relative
93 magnitudes of H^* of all the chemical species and that of SO_2 . Considering that the majority of the
94 chemical species are very reactive, a value of 1.0 was used for β for most species and smaller
95 values for a few less reactive species. α and β values were then adjusted based on the agreement
96 of nighttime V_d between modeled values and measured fluxes obtained from a forest site in the
97 southeastern US during summer (Nguyen et al., 2015). When adjusting α and β values, two rules
98 were first applied: (1) the trends in α (or β) values between different chemical species should be
99 consistent with the trends of their $\log(H^*)$ (or oxidizing capacity) (see Figure S1 for the finalized
100 α versus $\log(H^*)$); and (2) modeled mean and median nighttime V_d should be mostly within a
101 factor of 2.0 of the measured values (see discussion in Section 3.2 below). Only after these two
102 rules were satisfied, then the possible maximum α and β values were chosen to reduce the gap
103 between the modeled and measured daytime V_d , knowing that model predicted V_d were mostly
104 lower than the measured ones. Model theory and field data used for model evaluation are briefly
105 described below.

106

107 *2.1. Parameterization scheme for V_d of oVOCs and HCN*

108 The gaseous dry deposition scheme of Zhang et al. (2003) (hereinafter referred to as the Model)
109 was originally designed to model V_d for 31 chemical compounds including 9 inorganic species and



110 22 organics. Formic acid (HCOOH) is the only oVOC species that is available in both the Model
111 and the flux measurement dataset used here (described in the next section). In this study, the Model
112 was extended to include 12 new oVOC species and HCN. Briefly, V_d is calculated according to:

$$113 \quad V_d(z) = (R_a(z) + R_b + R_c)^{-1}, \quad (1)$$

114 where R_a is the aerodynamic resistance, R_b the quasi-laminar sub-layer resistance, R_c the surface
115 resistance, and z the reference height above the vegetation. R_a and R_b can be estimated using the
116 conventional micrometeorological approaches based on similarity theory and the equations used
117 in the Model can be found in Wu et al. (2018). R_c is parameterized as:

$$118 \quad \frac{1}{R_c} = \frac{1 - W_{st}}{R_s + R_m} + \frac{1}{R_{ns}}, \quad (2)$$

$$119 \quad \frac{1}{R_{ns}} = \frac{1}{R_{ac} + R_g} + \frac{1}{R_{cut}}, \quad (3)$$

120 where R_s is the canopy stomatal resistance, R_m the mesophyll resistance, R_{ns} the non-stomatal
121 resistance including resistance for uptake by leaf cuticles (R_{cut}) and by soil or ground litter (R_g),
122 R_{ac} in-canopy aerodynamic resistance, and W_{st} the fraction of stomatal blocking under wet
123 conditions.

124 R_s for any gaseous oVOCs (i) or HCN is also calculated using the sunlit/shade stomatal
125 resistance approach as was done in Zhang et al. (2002):

$$126 \quad \frac{1}{R_{s,i}} = G_s(PAR) f(T) f(D) f(\Psi) \frac{D_i}{D_{H_2O}}. \quad (4)$$

127 Here $G_s(PAR)$ is the unstressed canopy stomatal conductance for water vapor, a function of
128 photosynthetically active radiation (PAR). The dimensionless functions $f(T)$, $f(D)$ and $f(\psi)$ range
129 from 0 to 1, representing the fractional degree of stomatal closure caused by the stress from



130 temperature, water vapor pressure deficit, and leaf water potential, respectively. D_{H_2O} and D_i are
131 the molecular diffusivities for water vapor and the gas of interest, respectively.

132 R_{cut} and R_g for any oVOCs or HCN are scaled to those of SO_2 and O_3 with two species (i)-
133 dependent scaling parameters $\alpha(i)$ and $\beta(i)$:

$$134 \quad \frac{1}{R_{cut/g}(i)} = \frac{\alpha(i)}{R_{cut/g}(SO_2)} + \frac{\beta(i)}{R_{cut/g}(O_3)}. \quad (5)$$

135 $\alpha(i)$ and $\beta(i)$ values for all the chemical species are listed in Table 1, which are assigned using the
136 method described above.

137 The R_m for HCN was set to 100 s m^{-1} based on its effective Henry's law constants and
138 oxidizing capacities. Karl et al. (2010) found that enzymatic conversion can be an efficient pathway
139 for the immobilization of oVOCs (e.g., methacrolein and methyl vinyl ketone, acetaldehyde,
140 methacrolein) within leaf interior, besides dissolution and oxidation, which suggests that the
141 magnitude of R_m for oVOCs is minimal. Thus, the R_m for the oVOCs was set to 0 s m^{-1} (Table 1).

142

143 2.2. Field flux data

144 The fluxes of 16 atmospheric compounds (including 13 oVOC species, HCN, hydrogen peroxide
145 (H_2O_2), and nitric acid (HNO_3)) were measured using the eddy covariance (EC) technique at the
146 Centreville ("CTR") Southeastern Aerosol Research and Characterization Study (SEARCH) site
147 (hereinafter referred to as CTR). The CTR site (Brent, Alabama; 32.90°N , 87.25°W) is surrounded
148 by a grassy field to the south and a temperate mixed forest that is part of the Talladega National
149 Forest in all the other directions. The forest canopy is comprised of needleleaf coniferous (shortleaf,
150 longleaf, and loblolly pine; ~40%) and broadleaf deciduous (primarily oak, sweetgum, and hickory;
151 ~60%) tree species. A 20 m metal walk-up tower is used as the main structure supporting



152 instruments that measured the eddy covariance fluxes and related meteorological variables. The
153 sonic anemometer and the gas inlet were mounted at a height of about 22 m, facing north toward
154 the forest. The canopy height near the tower is on average ~10 m with a leaf area index (LAI) of
155 ~4.7 m² m⁻². A database of half-hourly V_d for 16 atmospheric compounds covering 5 non-
156 continuous days in June 2013 was obtained at the site. During these periods, the predominant winds
157 were northerly which is ideal to sample air from the forest (Figure S2) and the requirement on
158 energy balance closure was met (see Nguyen et al. (2015)). At CTR, it was typically humid (RH
159 50-80%) and warm (28-30 °C) in the daytime during the experiment (Figure S3). A comprehensive
160 description of the V_d dataset, data processing protocols, the instrumental methods, uncertainty
161 analysis, and the site characterizations can be found in Nguyen et al. (2015).

162

163 **3. Results and Discussion**

164 *3.1. Comparison of modeled resistance components*

165 *3.1.1. Atmospheric resistances (R_a and R_b)*

166 For very reactive and soluble substances such as HNO₃ and H₂O₂, R_c is often assumed to be close
167 to 0 (Hall & Claiborn, 1997; Meyers et al., 1989; Valverde-Canossa et al., 2006; Wesely & Hicks,
168 2000). The analysis of the measurement data showed that the daytime averaged V_d for HNO₃ and
169 H₂O₂ fitted well the rate of deposition without surface resistance ($V_d = 1/[R_a+R_b]$) (Nguyen et al.,
170 2015), which supports the assumption of near zero R_c for HNO₃ and H₂O₂ over the mixed
171 deciduous-coniferous CTR site under humid environment. Therefore, the measured V_d of HNO₃
172 and H₂O₂ can be used to evaluate the modeled atmospheric resistances for those species (the sum
173 of R_a and R_b). R_a represents the resistance for turbulent transport between the reference height and



174 the surface and is not chemical compound specific. R_b quantifies the resistance for the mass transfer
175 across the thin layer of air in contact with surface elements and is a function of the molecular
176 diffusivity of a specific compound (Wesely & Hicks, 1977). In theory, the differences in R_b
177 between any two gaseous species are only determined by differences in their molecular diffusivity
178 at any given turbulent condition.

179 Figure 1 compares the modeled average diel variations of V_d for HNO_3 and H_2O_2 against
180 observations. The measured V_d for HNO_3 and H_2O_2 peaked around noon at about 4 cm s^{-1} and 6
181 cm s^{-1} , respectively, and were less than 1 cm s^{-1} during the night. The model reproduced the diel
182 pattern and captured the peak V_d values at noon well. During the early night time (hours 19-23),
183 the modeled V_d for HNO_3 and H_2O_2 were on the order of 1 cm s^{-1} , much higher than the
184 measurements ($<0.2 \text{ cm s}^{-1}$). During the night, R_a dominates atmospheric resistance as it is usually
185 much larger than R_b in magnitude. This discrepancy between the measurement and the model
186 during the early night could be due to the stability correction functions used in the R_a calculation
187 (the equations can be found in the article by Wu et al. (2018)) which is subject to large uncertainties
188 under nocturnal stable conditions (Högström, 1988). The measurements indicated that H_2O_2
189 deposited slightly faster than HNO_3 , and the model reproduces well, as shown in Figure 1. Modeled
190 R_b for H_2O_2 is always smaller than that for HNO_3 due to the smaller molecular weight and the larger
191 molecular diffusivity. Overall, the model was in good agreement with the measurements regarding
192 V_d for HNO_3 and H_2O_2 , implying that the parameterization for atmospheric resistances (R_a and R_b)
193 was reasonable for the site during the study period.

194

195 3.1.2. Stomatal resistance (R_s)



196 Over vegetative areas, gas molecules can exit and enter the leaf through the stomata by molecular
197 diffusion, similar to the leaf-air exchange of water vapor and CO₂. In dry deposition models, R_s
198 for water vapor is estimated using evapotranspiration stomatal submodels, an approach that is also
199 popular in the land surface and climate communities. R_s is extended to any gas species using the
200 ratio of molecular diffusivity of the species of interest to that of water vapor (Pleim & Ran, 2011;
201 Wesely & Hicks, 2000). Figure 2 compares the modeled canopy stomatal conductance ($G_s = 1/R_s$)
202 for water vapor against the observation-based estimates. The observation-based G_s was estimated
203 by using the inversion of the Penman-Monteith (P-M) equation (Monteith & Unsworth, 1990)
204 which calculates R_s for water vapor by using measured water vapor fluxes and related
205 meteorological data (e.g., humidity, temperature). The evaporation from soil water and liquid
206 water on the vegetation surfaces is usually a minor contribution to the total water vapor flux
207 observed above a forest canopy during summer daytime. It was assumed that 85% of the water
208 vapor flux originated from transpiration in this study, following that used in the study of
209 Turnipseed et al. (2006) at Duke Forest, North Carolina. Note that a value of 90% was used by
210 Clifton et al. (2017) at Harvard Forest, Massachusetts. The uncertainty of the calculated R_s related
211 with the uncertainty in water vapor flux portion (on an order of 10%) is much smaller than the
212 differences between the modeled and the observation-based stomatal conductance (by a factor of
213 two) as discussed below.

214 The model reproduced the basic diel pattern in G_s (i.e., highest values between 08:00 and
215 11:00) but the peak value is only about half of the observation-based values. The Jarvis stomatal
216 submodel (Jarvis, 1976) used in the Model is known for its linear dependence on the prescribed
217 minimum stomatal resistance ($R_{s,min}$), a term that is subject to large uncertainties (Kumar et al.,
218 2011; Wu et al., 2018; Wu et al., 2011). A series of tests conducted by iteratively adjusting the



219 $R_{s,min}$ values showed the modeled G_s to be in better agreement with observations if $R_{s,min}$ was
220 decreased by 40% (Figure 2). G_s from the Model with the adjusted $R_{s,min}$ was in good agreement
221 with the observation-based values for most of the time, though the modeled values were slightly
222 smaller than the observation-based estimates around noon. Analysis of the R_s parameterization
223 indicates that this discrepancy was related to the stress function for water vapor pressure deficit
224 (VPD) used in the Jarvis stomatal submodel, which may overpredict the stress on stomatal opening
225 due to high VPD around noon.

226

227 3.1.3. Non-stomatal resistance (R_{ns})

228 To assess if the non-stomatal resistance (R_{ns}) parametrization (Eq. 3) is reasonable, modeled $1/R_{ns}$
229 (defined as G_{ns}) values are compared with the non-stomatal portion of the flux, the inverse of
230 which is termed the residual conductance ($G_{residual}$). $G_{residual}$ includes all processes influencing
231 deposition aside from R_a , R_b , R_m , and R_s , calculated as $[V_d^{-1} - (R_a + R_b)]^{-1} - (R_s + R_m)^{-1}$. Here V_d is
232 from the observations, R_a and R_b are calculated using the Model driven by the observed
233 meteorology, R_s is the observation-based estimates by the P-M method, adjusted by the molecular
234 diffusivity of each gas (similar to Eq. 4), and R_m is listed in Table 1. Although considerable
235 uncertainties in the calculated $G_{residual}$ exist (in this form of back-calculation, we must assume that
236 the G_{ns} terms are correctly estimated), it can provide useful information on the flux/ V_d resulting
237 from processes such as deposition to the leaf cuticle and ground (i.e., non-stomatal) or chemical
238 loss due to reactions within and near the canopy that lead to flux divergence.

239 Figure 3 compares the observation-based $G_{residual}$ for each oVOC species or HCN against
240 the corresponding modeled non-stomatal conductance (G_{ns}) under different conditions. The mean
241 and median values are presented in Table S3. During the nighttime when the canopy surface was



242 dry (no dew), the $G_{residual}$ for oVOC species ranged from 0.08 to 0.18 cm s^{-1} and the modeled G_{ns}
243 was comparable in magnitude. When the surface was wet from dew formation on leaves and
244 needles, the oVOC species showed an increase in $G_{residual}$ by 55%-440% compared to the nighttime
245 dry surface. The model captured the increases in non-stomatal uptake when the surface become
246 wet with dew, although it may underestimate (e.g., HDC₄, INP, HCN) or overestimate (e.g., PAA,
247 DHC₄, HCOOH) the wetness effects. During the daytime of the study period, no precipitation was
248 recorded at the CTR site (Figure S3) and the canopy surface was dry. The mean $G_{residual}$ for oVOCs
249 ranged from 0.5 cm s^{-1} to 8.7 cm s^{-1} during the daytime, much higher than the modeled G_{ns} for most
250 species (0.2 - 1 cm s^{-1}). Figure S4 presents the diel variations of $G_{residual}$ and G_{ns} and it shows that
251 the modeled G_{ns} showed smaller diel variations than those of $G_{residual}$ and large differences in
252 magnitude can be seen during the daytime. The modeled G_{ns} showed a peak during the early
253 morning (around 7:00) which may be due to the enhanced non-stomatal uptake by dew wetted
254 surfaces.

255

256

257 3.2. Evaluation of modeled deposition velocities

258 Figure 4 shows model-measurement comparison of diel V_d of the oVOCs and HCN and Table 2
259 presents the statistical results of the comparison. As described in Section 2, the assigned α and β
260 values should first produce reasonable nighttime V_d . Modeled nighttime mean V_d were very close
261 to measurements for the majority of the chemical species, although the differences were somewhat
262 larger for the median values (Table 2). Three species (HAC, HPALD, PROPNN) still had 50%
263 lower modeled than measured nighttime mean V_d , but have slightly higher modeled than measured
264 nighttime median V_d . In contrast, modeled daytime mean V_d were more than 50% lower than the



265 measured values for four species (HMHP, PAA, HPALD, ISOPOOH/IEPOX) and were also
266 significantly lower for several other species. Only three species (MTNP, HCN, HCOOH) had
267 comparable modeled and measured V_d for both day- and nighttime. One species (DHC₄) had
268 slightly lower of modeled than measured daytime mean or median V_d , but with an opposite trend
269 for nighttime V_d .

270 The model reproduced the basic features of the diurnal pattern of the observations, showing
271 highest values during the day and lowest values at night. Correlation coefficients between the
272 measurement and the model ranged from 0.52 to 0.77. At night, the measured V_d for the oVOCs
273 remained relatively low, typically ranging from 0.1-0.5 cm s⁻¹, and the model produced the same
274 magnitudes for most of the species. During the daytime, the model can only capture the magnitudes
275 of the measured V_d for a few species (e.g., HCN, HCOOH, MTNP, DHC₄), of which the peak V_d
276 values were less than 1.5 cm s⁻¹. For the other species, the measured peak V_d values were in the
277 range of 2 to 5 cm s⁻¹, while the modeled results were below 1 cm s⁻¹. As shown in section 3.1.2,
278 the modeled G_s was likely underestimated when compared to the simultaneous measurements of
279 water vapor flux. Adjusting G_s higher by 67% (through reducing $R_{s,min}$ by 40%) can only increase
280 the modeled V_d of the oVOCs by 10-40% during the daytime (see the sensitivity test in Figure 4),
281 and the peak values were still mostly below 1 cm s⁻¹. Figure 5 shows that the model captured the
282 differences in measured V_d for the oVOCs to some extent. The model-measurement agreements
283 were good for species with the measured mean V_d below 0.5 cm s⁻¹, above which the discrepancy
284 increased. For the measurements, the mean values were significantly larger than the median values,
285 especially for the fast-deposited species, indicating that the distribution of the measured V_d values
286 skewed to the right (high values). The model has a better agreement with the measurements by
287 comparing the median versus mean values.



288 At night when stomata are mostly closed and atmospheric chemical reactions are largely
289 inhibited, the measured fluxes above the canopy should better represent non-stomatal surface
290 uptake. In the presence of sunlight, fast chemical reactions between the inlet and canopy could
291 make a significant or even dominant contribution to the measured fluxes of reactive species
292 (Farmer & Cohen, 2008; Wolfe et al., 2011). The impact of fast chemical reactions on surface
293 fluxes should be different for different chemical species. To verify this hypothesis, two chemical
294 species (HAC and PAA) having similar molecular weights (74 Da and 76 Da, respectively) but
295 very different daytime fluxes were compared (Figure 6). Their similar molecular diffusivities
296 (controlled by molecular weight) suggest that they should be transferred through the quasi-laminar
297 sub-layer and taken up through leaf stomata at similar rates, resulting in similar resistance
298 components of R_b and R_s . Note that R_a is universal to any trace gases and R_m is assumed to be
299 negligible. Thus, the differences between their V_d should be caused by their different non-stomatal
300 sinks. At night, V_d values were similar between HAC and PAA (median values: 0.04 cm s^{-1}) over
301 dry surfaces. When the surfaces were wet due to dew formation, V_d for both HAC and PAA
302 increased (median values: $0.30\text{-}0.48 \text{ cm s}^{-1}$). In contrast, $V_d(\text{PAA})$ was much higher than $V_d(\text{HAC})$
303 during daytime, suggesting additional or larger sinks exist for PAA compared to HAC. Thus, fast
304 chemical processing and subsequent flux divergence above the canopy likely caused the large
305 discrepancies between the measured and modeled V_d for the reactive oVOC compounds during the
306 daytime.

307 Chemical processes indeed can cause flux divergence or convergence at the surface, which
308 has been supported by growing evidence from field measurements (e.g., Farmer and Cohen, 2008;
309 Min et al., 2014; Wolfe et al. 2009). For example, Wolfe et al. (2009) suggested that the differences
310 in loss rate between the inlet and canopy may be an important contributor to the measured net flux



311 of peroxyacetyl nitrate, irrespective of turbulent timescales. Photochemical OH production is
312 reduced within canopies, which in turn slows down the oxidation of volatile organic compounds
313 and the photolysis of organic nitrates. The oVOCs measured at the CTR site are mainly produced
314 from the oxidation of isoprene and monoterpenes (Nguyen et al., 2015). Most of the oVOCs are
315 quite chemically reactive and can undergo fast oxidation (e.g., multifunctional carbonyls),
316 decomposition (e.g., HMHP), or photolysis (e.g., organic nitrates) (Müller et al., 2014; Nguyen et
317 al., 2015). Vertical gradients in the chemical production and loss rates below the inlet can exhibit
318 chemical flux divergence, which contributes to the net flux above canopy. Quantifying the effects
319 of chemical processing on the net flux would require a multi-layer model with resolved emission,
320 deposition, turbulent diffusion, and chemical processes throughout the canopy, which is
321 recommended for future studies (e.g., Ashworth et al., 2015; Bryan et al., 2012; Stroud et al., 2005;
322 Wolfe & Thornton, 2011; Zhou et al., 2017).

323 Quantifying V_d as the ratio of flux to concentration at one measurement height only ($V_d =$
324 F/C_x), rather than as the ratio of flux to the concentration difference at the measurement height
325 and the surface ($V_d = F/[C_x - C_0]$), although commonly employed in analyzing eddy covariance
326 flux measurements, is a simplification. It is valid for 1) matter that disappears nearly completely
327 by reactions at the surface, and 2) unstable or neutral conditions. Most chemical species considered
328 here may satisfy the first condition. With regards to the second condition, our analysis is based on
329 the assumption that, under stable conditions at nighttime, concentrations observed at the
330 measurement height change in relation to the fluxes measured at this height. However, no relation
331 between measured concentration and flux is typically observed due to the presence of a shallow
332 stable boundary layer, connection between the stable free atmosphere and stable boundary layer
333 by internal gravity waves, ground inversions, and low-level jets, leading to intermittent turbulence



334 at the measurement height containing a gravity wave signal, and non-steady-state conditions
335 (Foken, 2017). Future efforts to model oVOC and HCN deposition velocities above forest canopies
336 should be based on neutral or unstable boundary layer flux measurements only, or, for example,
337 on modified Bowen ratio flux measurement in which concentrations are measured at two heights
338 in the constant flux layer. Such an approach can provide a means to compute a measured deposition
339 velocity of a surface reactive substance as proportional to the ratio between the measured flux and
340 the measured concentration difference.

341

342 **4. Summary and recommendations**

343 The number of chemical species simulated in chemical transport models (CTMs) has been
344 increasing with increasing computer power. Among these, oVOCs and HCN are an important
345 groups of atmospheric pollutants for which dry deposition processes need to be treated as
346 accurately as possible, so that their inputs to ecosystems (noting that some oVOCs are organic
347 nitrogen) and their roles on other atmospheric chemistry processes (e.g., formation of ozone and
348 secondary organic aerosols) can be assessed. Earlier dry deposition schemes have considered very
349 few oVOCs and need to be extended for more species. Dry deposition of HCN was assumed to be
350 negligible in some CTMs (e.g., Moussa et al., 2016). The present study first generated effective
351 Henry's law constant and oxidizing capacity, the two key physical and chemical properties that
352 are considered to control the dry deposition process (Wesely & Hicks, 2000), for 12 oVOCs
353 species and HCN. Two scaling factors for the non-stomatal resistance and one for the mesophyll
354 resistance were applied to individual oVOCs and HCN for calculating their respective V_d .

355 The modeled nighttime V_d agrees well with the measured data for most of the oVOCs,
356 suggesting that the current non-stomatal parameterization scheme is a reasonable approach. The



357 stomatal conductance for water vapor, with adjusted (reduced) $R_{s,min}$, also agrees well with
358 measured values. However, the modeled peak V_d values during daytime are only a fraction (0.2-
359 0.5) of the measured values for some of the oVOCs, suggesting that fast atmospheric chemical
360 processes likely contributed to the total measured fluxes. In practice, these additional fluxes during
361 daytime can be modeled as non-stomatal uptake and better model-measurement agreement can be
362 obtained by adjusting the non-stomatal parameterization scheme (e.g., Müller et al., 2018; Paulot
363 et al., 2018). However, using this approach will produce unreasonably high values for the solubility
364 parameter and overpredict V_d during nighttime if the same non-stomatal formulas are used for both
365 day and nighttime (as is the case in the existing schemes). More importantly, the high measured
366 V_d have only been observed at relatively few sites during very short periods (Karl et al., 2010;
367 Nguyen et al., 2015). More evidence is needed to parameterize V_d for oVOCs to different land use
368 categories over entire seasons. Until then, the conservative estimates of V_d such as modeled in this
369 study are still recommended for use in chemical transport models. The model parameters chosen
370 for V_d of these oVOCs provide the best-known representation of their respective physicochemical
371 properties, and the modelled V_d values fall within the range of the low-end values of the available
372 measurements.

373 Future field studies should focus on conducting flux measurements of oVOC compounds
374 with highest uncertainties, such as those that are most chemically reactive in the atmosphere or
375 most rapidly taken up by wet surfaces. Additional measurements are also needed in different
376 ecosystems to inform the representativeness of the high oVOC V_d reported by Nguyen et al. (2015)
377 and Karl et al. (2010). Furthermore, concurrent chemical measurements of oxidants such as O_3 and
378 radicals are needed to quantify flux divergence due to fast within-and near-canopy chemical
379 reactions. Future dry deposition schemes should include additional biochemical processes and



380 species-dependent parameters for non-stomatal uptake, including enzymatic reactions (Karl et al.,
381 2010), the octanol-air partitioning coefficients to account for the cavity formation and polar
382 intermolecular interactions with leaf surfaces and reservoirs (Nizzetto and Perlinger, 2012), and
383 the enhancement/reduction effects due to soil and leaf moisture. Chemical processes within the
384 canopy airspace could also be coupled with emission and deposition schemes to realistically
385 simulate chemicals fate and transport, including bi-directional fluxes of reactive compounds
386 discussed here, as well as less reactive compounds such as methanol. Such an approach would
387 require specification of chemical conditions within and near the canopy as well as in-canopy
388 radiation and air flow. While more computationally intensive, the results presented here reinforce
389 the need for such advanced models to explicitly resolve the non-stomatal processes contributing
390 to the net atmosphere-biosphere exchange of reactive compounds. Above all, intercomparison
391 studies should be first conducted for existing models that can handle oVOC dry deposition
392 processes to quantify the magnitudes of uncertainties in the simulated V_d as well as the associated
393 ambient concentration and deposition fluxes.

394 **Code and data availability**

395 The computer code and data used in this study can be obtained from containing the corresponding
396 author.

397 **Competing interests**

398 The authors declare that they have no conflict of interest.

399 **Author contributions**

400 ZW conducted model run and data analysis and drafted the manuscript. LZ designed the project,
401 finalized computer code, drafted part of the manuscript and finalized the paper. JTW contributed



402 to manuscript writing and commented on the manuscript. PAM generated chemistry data that are
403 used in the supporting document and commented on the manuscript. JAP contributed to model
404 design and manuscript writing and commented on the manuscript. XW contributed to the project
405 design and commented on the manuscript.

406

407 **Acknowledgments**

408 We thank Tran Nguyen for the field flux data and Glenn Wolfe and Christopher Groff for the tree
409 survey data. We also greatly appreciate helpful comments from Tran Nguyen, Chris Geron and
410 Donna Schwede. X. Wang was supported by the Chinese National Key Research and Development
411 Plan (2017YFC0210100) and the State Key Program of National Natural Science Foundation of
412 China (91644215). The SouthEastern Aerosol Research and CHaracterization (SEARCH) network
413 was sponsored by the Southern Company and the Electric Power Research Institute. The field data
414 during the SOAS 2013 campaign is available at
415 <https://esrl.noaa.gov/csd/groups/csd7/measurements/2013senex/Ground/DataDownload/>.

416 *Disclaimer: The research presented was not performed or funded by U.S. Environmental*
417 *Protection Agency and was not subject to EPA's quality system requirements. The views expressed*
418 *in this article are those of the authors and do not necessarily represent the views or policies of the*
419 *U.S. Environmental Protection Agency.*

420

References:

421 Ashworth, K., Chung, S., Griffin, R., Chen, J., Forkel, R., Bryan, A., et al. (2015). FORest Canopy
422 Atmosphere Transfer (FORcAsT) 1.0: a 1-D model of biosphere–atmosphere chemical exchange.
423 *Geoscientific Model Development*, 8(11), 3765–3784.



- 424 Bryan, A., Bertman, S., Carroll, M., Dusanter, S., Edwards, G., Forkel, R., et al. (2012). In-canopy gas-
425 phase chemistry during CABINEX 2009: sensitivity of a 1-D canopy model to vertical mixing and
426 isoprene chemistry. *Atmospheric Chemistry and Physics*, 12(18), 8829-8849.
- 427 Bunkan, A.J.C., Liang, C.-H., Pilling, M.J., & Nielsen, C.J. (2013). Theoretical and experimental study of the
428 OH radical reaction with HCN. *Molecular Physics*, 111 (9-11), 1589-1598.
- 429 Clifton, O. E., Fiore, A. M., Munger, J., Malyshev, S., Horowitz, L., Shevliakova, E., et al. (2017).
430 Interannual variability in ozone removal by a temperate deciduous forest. *Geophysical Research*
431 *Letters*, 44(1), 542-552.
- 432 Farmer, D., & Cohen, R. (2008). Observations of HNO₃, ΣAN, ΣPN and NO₂ fluxes: Evidence for rapid HO_x
433 chemistry within a pine forest canopy. *Atmospheric Chemistry and Physics*, 8(14), 3899-3917.
- 434 Flechard, C., Nemitz, E., Smith, R., Fowler, D., Vermeulen, A., Bleeker, A., et al. (2011). Dry deposition of
435 reactive nitrogen to European ecosystems: a comparison of inferential models across the
436 NitroEurope network. *Atmospheric Chemistry and Physics*, 11(6), 2703-2728.
- 437 Foken, T. (2017). *Micrometeorology*, 2nd ed., Springer, pp. 105-151.
- 438 Hall, B. D., & Claiborn, C. S. (1997). Measurements of the dry deposition of peroxides to a Canadian
439 boreal forest. *Journal of Geophysical Research: Atmospheres*, 102(D24), 29343-29353.
- 440 Högström, U. (1988). Non-dimensional wind and temperature profiles in the atmospheric surface layer:
441 A re-evaluation. *Boundary-Layer Meteorology*, 42, 55-78.
- 442 Jarvis, P. (1976). The interpretation of the variations in leaf water potential and stomatal conductance
443 found in canopies in the field. *Philosophical Transactions of the Royal Society of London B:*
444 *Biological Sciences*, 273(927), 593-610.
- 445 Karl, T., Harley, P., Emmons, L., Thornton, B., Guenther, A., Basu, C., et al. (2010). Efficient atmospheric
446 cleansing of oxidized organic trace gases by vegetation. *Science*, 330(6005), 816-819.
- 447 Kelly, J. M., Doherty, R. M., O'Connor, F. M., Mann, G. W., Coe, H., & Liu, D. (2019). The roles of volatile
448 organic compound deposition and oxidation mechanisms in determining secondary organic
449 aerosol production: A global perspective using the UKCA chemistry-climate model (vn8. 4).
450 *Geoscientific Model Development*, 12, 2539–2569.
- 451 Kumar, A., Chen, F., Niyogi, D., Alfieri, J. G., Ek, M., & Mitchell, K. (2011). Evaluation of a photosynthesis-
452 based canopy resistance formulation in the Noah land-surface model. *Boundary-Layer*
453 *Meteorology*, 138(2), 263-284.
- 454 Meyers, T., Huebert, B., & Hicks, B. (1989). HNO₃ deposition to a deciduous forest. *Boundary-Layer*
455 *Meteorology*, 49(4), 395-410.
- 456 Min, K., Pusede, S., Browne, E., LaFranchi, B. & Cohen, R. (2014). Eddy covariance fluxes and vertical
457 concentration gradient measurements of NO and NO₂ over a ponderosa pine ecosystem:
458 observational evidence for within-canopy chemical removal of NO_x. *Atmospheric Chemistry and*
459 *Physics*, 14(11), 5495-5512.
- 460 Monteith, J. L., & Unsworth, M. (1990). *Principles of Environmental Physics* (2nd ed.). London:
461 Butterworth-Heinemann.
- 462 Moussa, S. G., Leithead, A., Li, S.-M., Chan, T. W., Wentzell, J. J., Stroud, C., Zhang, J., Lee, P., Lu, G., &
463 Brook, J. R. (2016). Emissions of hydrogen cyanide from on-road gasoline and diesel vehicles.
464 *Atmospheric Environment*, 131, 185-195.
- 465 Müller, J. F., Peeters, J., & Stavrou, T. (2014). Fast photolysis of carbonyl nitrates from isoprene.
466 *Atmospheric Chemistry and Physics*, 14(5), 2497-2508. doi:10.5194/acp-14-2497-2014
- 467 Müller, J. F., Stavrou, T., Bauwens, M., Compornolle, S., & Peeters, J. (2018). Chemistry and deposition
468 in the Model of Atmospheric composition at Global and Regional scales using Inversion
469 Techniques for Trace gas Emissions (MAGRITTE v1.0). Part B. Dry deposition. *Geoscientific Model*
470 *Development Discussion*, 2018, 1-49. doi:10.5194/gmd-2018-317



- 471 Nguyen, T. B., Crouse, J. D., Teng, A. P., Clair, J. M. S., Paulot, F., Wolfe, G. M., et al. (2015). Rapid
472 deposition of oxidized biogenic compounds to a temperate forest. *Proceedings of the National*
473 *Academy of Sciences*, 112(5), E392-E401.
- 474 Nizzetto, L. & Perlinger, J.A. (2012). Climatic, biological, and land cover controls on the exchange of gas-
475 phase semivolatile chemical pollutants between forest canopies and the atmosphere.
476 *Environmental Science & Technology*, 46(5), 2699-2707.
- 477 Paulot, F., Malyshev, S., Nguyen, T., Crouse, J. D., Shevliakova, E., & Horowitz, L. W. (2018).
478 Representing sub-grid scale variations in nitrogen deposition associated with land use in a global
479 Earth system model: implications for present and future nitrogen deposition fluxes over North
480 America. *Atmospheric Chemistry and Physics*, 18(24), 17963-17978.
- 481 Pleim, J., & Ran, L. (2011). Surface flux modeling for air quality applications. *Atmosphere*, 2(3), 271-302.
- 482 Pye, H. O., Luecken, D. J., Xu, L., Boyd, C. M., Ng, N. L., Baker, K. R., et al. (2015). Modeling the current
483 and future roles of particulate organic nitrates in the southeastern United States. *Environmental*
484 *Science & Technology*, 49(24), 14195-14203.
- 485 Silva, S. J., & Heald, C. L. (2018). Investigating dry deposition of ozone to vegetation. *Journal of*
486 *Geophysical Research: Atmospheres*, 123(1), 559-573.
- 487 Singh, H.B., Salas, L., Herlth, D., Kolyer, R., Czech, E., Viezee, W., et al. (2003). In situ measurements of
488 HCN and CH₃CN over the Pacific Ocean: sources, sinks, and budgets. *Journal of Geophysical*
489 *Research: Atmospheres*, 108(D20), 8795.
- 490 Stroud, C., Makar, P., Karl, T., Guenther, A., Geron, C., Turnipseed, A., et al. (2005). Role of canopy -
491 scale photochemistry in modifying biogenic - atmosphere exchange of reactive terpene species:
492 Results from the CELTIC field study. *Journal of Geophysical Research: Atmospheres*, 110(D17).
- 493 Turnipseed, A., Huey, L., Nemitz, E., Stickel, R., Higgs, J., Tanner, D., et al. (2006). Eddy covariance fluxes
494 of peroxyacetyl nitrates (PANs) and NO_y to a coniferous forest. *Journal of Geophysical Research:*
495 *Atmospheres*, 111(D9).
- 496 Valverde-Canossa, J., Ganzeveld, L., Rappenglück, B., Steinbrecher, R., Klemm, O., Schuster, G., et al.
497 (2006). First measurements of H₂O₂ and organic peroxides surface fluxes by the relaxed eddy-
498 accumulation technique. *Atmospheric Environment*, 40, 55-67.
- 499 Wesely, M. (1989). Parameterization of surface resistances to gaseous dry deposition in regional-scale
500 numerical models. *Atmospheric Environment*, 23(6), 1293-1304.
- 501 Wesely, M., & Hicks, B. (1977). Some factors that affect the deposition rates of sulfur dioxide and similar
502 gases on vegetation. *Journal of the Air Pollution Control Association*, 27(11), 1110-1116.
- 503 Wesely, M., & Hicks, B. (2000). A review of the current status of knowledge on dry deposition.
504 *Atmospheric Environment*, 34(12), 2261-2282.
- 505 Wolfe, G., & Thornton, J. (2011). The chemistry of atmosphere-forest exchange (CAFÉ) model—Part 1:
506 Model description and characterization. *Atmospheric Chemistry and Physics*, 11(1), 77-101.
- 507 Wolfe, G., Thornton, J., McKay, M., & Goldstein, A. (2011). Forest-atmosphere exchange of ozone:
508 sensitivity to very reactive biogenic VOC emissions and implications for in-canopy
509 photochemistry. *Atmospheric Chemistry and Physics*, 11(15), 7875-7891.
- 510 Wolfe, G., Thornton, J., Yatavelli, R., McKay, M., Goldstein, A., LaFranchi, B., et al. (2009). Eddy
511 covariance fluxes of acyl peroxy nitrates (PAN, PPN and MPAN) above a Ponderosa pine forest.
512 *Atmospheric Chemistry and Physics*, 9, 615–635.
- 513 Wright, L. P., Zhang, L., Cheng, I., Aherne, J., & Wentworth, G. R. (2018). Impacts and Effects Indicators
514 of Atmospheric Deposition of Major Pollutants to Various Ecosystems-A Review. *Aerosol and Air*
515 *Quality Research*, 18, 1953-1992.
- 516 Wu, Z. Y., Schwede, D. B., Vet, R., Walker, J. T., Shaw, M., Staebler, R., et al. (2018). Evaluation and
517 intercomparison of five North American dry deposition algorithms at a mixed forest site. *Journal*
518 *of Advances in Modeling Earth Systems*, 10(7), 1571-1586.



- 519 Wu, Z. Y., Wang, X. M., Chen, F., Turnipseed, A. A., Guenther, A. B., Niyogi, D., et al. (2011). Evaluating
520 the calculated dry deposition velocities of reactive nitrogen oxides and ozone from two
521 community models over a temperate deciduous forest. *Atmospheric Environment*, 45(16), 2663-
522 2674.
- 523 Wu, Z. Y., Wang, X. M., Turnipseed, A. A., Chen, F., Zhang, L. M., Guenther, A. B., et al. (2012). Evaluation
524 and improvements of two community models in simulating dry deposition velocities for
525 peroxyacetyl nitrate (PAN) over a coniferous forest. *Journal of Geophysical Research -
526 Atmospheres*, 117, D04310.
- 527 Wu, Z. Y., Zhang, L., Wang, X. M., & Munger, J. W. (2015). A modified micrometeorological gradient
528 method for estimating O₃ dry depositions over a forest canopy. *Atmospheric Chemistry and
529 Physics*, 15(13), 7487-7496.
- 530 Xie, Y., Paulot, F., Carter, W., Nolte, C., Luecken, D., Hutzell, W., et al. (2013). Understanding the impact
531 of recent advances in isoprene photooxidation on simulations of regional air quality.
532 *Atmospheric Chemistry and Physics*, 13(16), 8439-8455.
- 533 Zhang, L., Brook, J., & Vet, R. (2003). A revised parameterization for gaseous dry deposition in air-quality
534 models. *Atmospheric Chemistry and Physics*, 3(6), 2067-2082.
- 535 Zhang, L., Moran, M. D., Makar, P. A., Brook, J. R., & Gong, S. (2002). Modelling gaseous dry deposition
536 in AURAMS: a unified regional air-quality modelling system. *Atmospheric Environment*, 36(3),
537 537-560.
- 538 Zhou, P., Ganzeveld, L., Taipale, D., Rannik, Ü., Rantala, P., Rissanen, M. P., et al. (2017). Boreal forest
539 BVOC exchange: emissions versus in-canopy sinks. *Atmospheric Chemistry and Physics*, 17(23),
540 14309-14332.



Table 1. List of model parameters needed in the scheme of Zhang et al. (2003) for simulating dry deposition velocity of additional oVOCs species and HCN: α and β are scaling parameters for non-stomatal resistance, and R_m is mesophyll resistance.

Symbol	Name	Molecular Weight (Da)	Scaling Parameters		R_m (s m ⁻¹)
			α	β	
HMHP	hydroxymethyl hydroperoxide	64	5	1	0
HAC	hydroxyacetone	74	1.5	1	0
PAA	peroxyacetic acid	76	2	1	0
HDC ₄	the C4 hydroxy dicarbonyl from IEPOX oxidation	102	1	0.2	0
DHC ₄	the C4 dihydroxy carbonyl from IEPOX oxidation	104	2	0.2	0
HPALD	isoprene hydroperoxy aldehydes	116	1.5	1	0
ISOPOOH/IEPOX ^a	isoprene hydroxyhydroperoxide and isoprene dihydroxyepoxide	118	5	0.2	0
PROPNN	propanone nitrate or propanal nitrate	119	1.5	1	0
ISOPN	isoprene hydroxy nitrates	147	1.5	1	0
MACN/MVKN ^a	methacrolein and Methyl vinyl ketone hydroxy nitrate	149	1.5	1	0
INP	isoprene nitrooxy hydroperoxide	163	1.5	1	0
MTNP	monoterpene nitrooxy hydroperoxide	231	1.5	1	0
HCN	hydrogen cyanide	27	0	0.1	100
HCOOH ^b	formic acid	46	2	0.2	0

^a Treated as one group of compounds in the field measurements due to instrument limitation and have the same parameter values in the model.

^b Beta value for HCOOH in Zhang et al. (2003) is 0.0, and here is given as 0.2 to be consistent to other oVOC species here (which would make no difference since the alpha value of 2 would dominate the nonstomatal resistance).



Table 2. Statistical results of the observed and modeled dry deposition velocity (V_d) for oVOCs and HCN (cm s^{-1})^a

Compound	All					Daytime				Nighttime		
	N	Obs	Mod	Mod- $R_{s,min}$	R	N	Obs	Mod	Mod- $R_{s,min}$	N	Obs	Mod
HMHP	247	1.66 (0.61)	0.69 (0.54)	0.75 (0.58)	0.63	85	3.42 (3.49)	1.05 (1.04)	1.19 (1.17)	128	0.33 (0.13)	0.37 (0.24)
HAC	245	0.84 (0.53)	0.41 (0.31)	0.49 (0.36)	0.61	84	1.21 (1.07)	0.65 (0.62)	0.81 (0.78)	128	0.44 (0.12)	0.21 (0.15)
PAA	243	1.08 (0.52)	0.46 (0.34)	0.53 (0.37)	0.74	85	2.18 (2.15)	0.71 (0.69)	0.86 (0.83)	128	0.28 (0.09)	0.24 (0.17)
HDC ₄	205	0.45 (0.22)	0.30 (0.20)	0.37 (0.23)	0.64	66	0.91 (0.78)	0.51 (0.49)	0.66 (0.65)	111	0.10 (0.06)	0.15 (0.10)
DHC ₄	247	0.42 (0.21)	0.41 (0.31)	0.47 (0.36)	0.61	85	0.92 (0.85)	0.63 (0.61)	0.76 (0.73)	128	0.08 (0.06)	0.22 (0.16)
HPALD	247	1.11 (0.46)	0.39 (0.29)	0.45 (0.34)	0.67	85	2.08 (2.17)	0.60 (0.58)	0.73 (0.70)	128	0.40 (0.10)	0.21 (0.15)
ISOPOOH/IEPOX	247	1.02 (0.49)	0.63 (0.48)	0.67 (0.52)	0.59	85	2.11 (2.06)	0.94 (0.94)	1.05 (1.05)	128	0.28 (0.09)	0.34 (0.23)
PROPNN	246	0.89 (0.43)	0.39 (0.29)	0.45 (0.33)	0.53	84	1.40 (1.38)	0.60 (0.58)	0.73 (0.70)	128	0.46 (0.13)	0.21 (0.15)
ISOPN	247	0.68 (0.39)	0.38 (0.28)	0.43 (0.33)	0.62	85	1.27 (1.29)	0.58 (0.57)	0.70 (0.67)	128	0.21 (0.09)	0.21 (0.15)
MACN/MVKN	246	0.65 (0.32)	0.38 (0.28)	0.43 (0.32)	0.57	84	1.19 (1.15)	0.58 (0.57)	0.70 (0.66)	128	0.22 (0.06)	0.21 (0.15)
INP	247	0.64 (0.46)	0.38 (0.28)	0.43 (0.33)	0.63	85	1.12 (1.17)	0.57 (0.56)	0.68 (0.65)	128	0.24 (0.10)	0.20 (0.15)
MTNP	246	0.33 (0.13)	0.36 (0.27)	0.40 (0.31)	0.54	84	0.55 (0.57)	0.54 (0.54)	0.64 (0.62)	128	0.16 (0.04)	0.20 (0.15)
HCN	234	0.13 (0.06)	0.17 (0.15)	0.22 (0.20)	0.77	84	0.26 (0.24)	0.33 (0.34)	0.43 (0.45)	117	0.03 (0.01)	0.03 (0.01)
HCOOH	244	0.47 (0.27)	0.46 (0.35)	0.54 (0.41)	0.52	83	0.82 (0.75)	0.72 (0.68)	0.91 (0.88)	127	0.20 (0.05)	0.23 (0.16)

^a Note: N is the number of samples; R is the correlation coefficient between observation (Obs) and model simulation (Mod); “Mod- $R_{s,min}$ ” refers to a sensitivity test in which $R_{s,min}$ was reduced by 40%; Daytime is 09:00-17:00 (local time) and nighttime is 20:00-06:00 (local time). Median values are provided in parentheses, following arithmetic mean values.

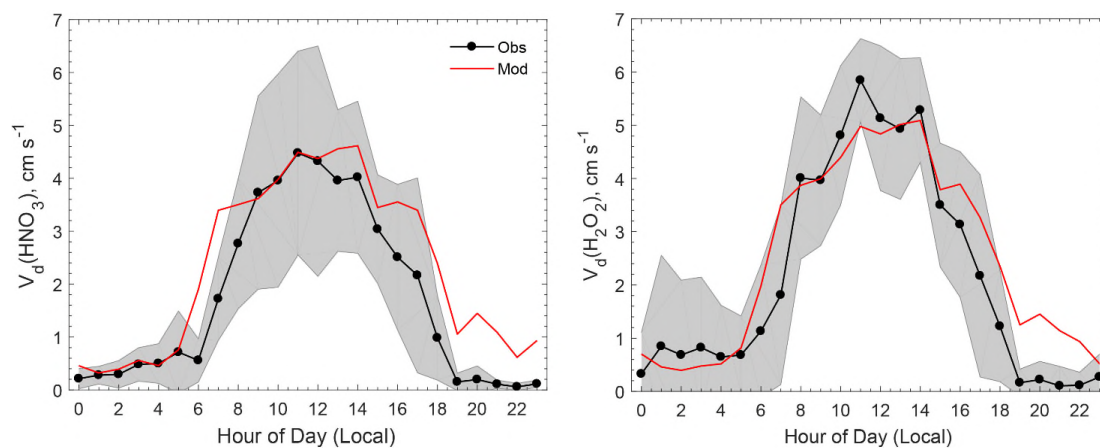


Figure 1. Comparison of the observed and modeled average diel variations of dry deposition velocities (V_d) for HNO_3 and H_2O_2 . The shaded area indicates the standard deviation of the observations. The model assumes that surface resistances (R_c) for HNO_3 and H_2O_2 are zero.

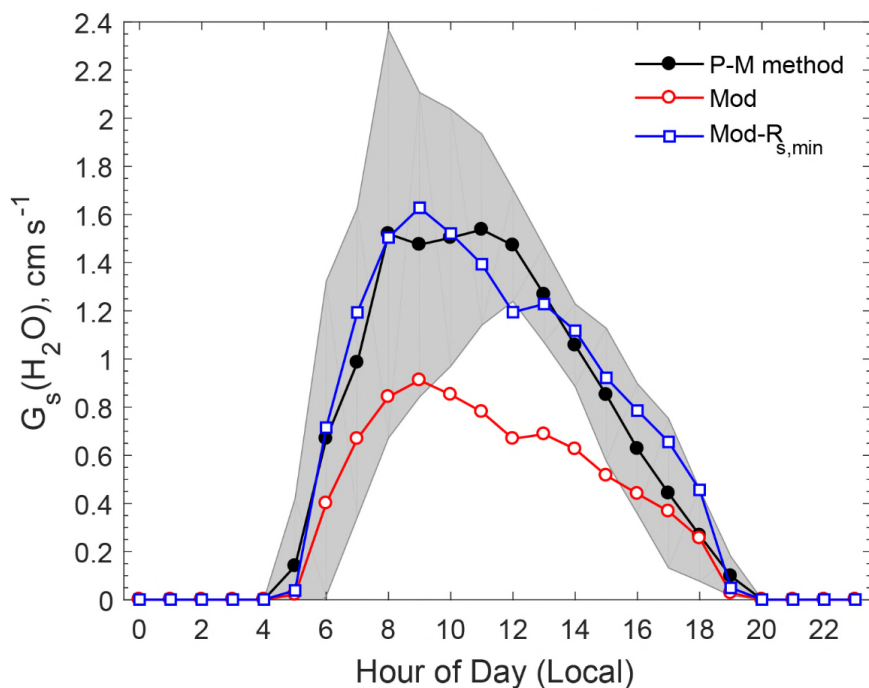


Figure 2. Comparison of observation-based and modeled averaged diel variations of stomatal conductance (G_s) for water vapor. The shaded area indicates the standard deviation of the observation-based $G_s(H_2O)$ estimated by the P-M method. “Mod- $R_{s,min}$ ” refers to a model sensitivity test in which $R_{s,min}$ was reduced by 40%.

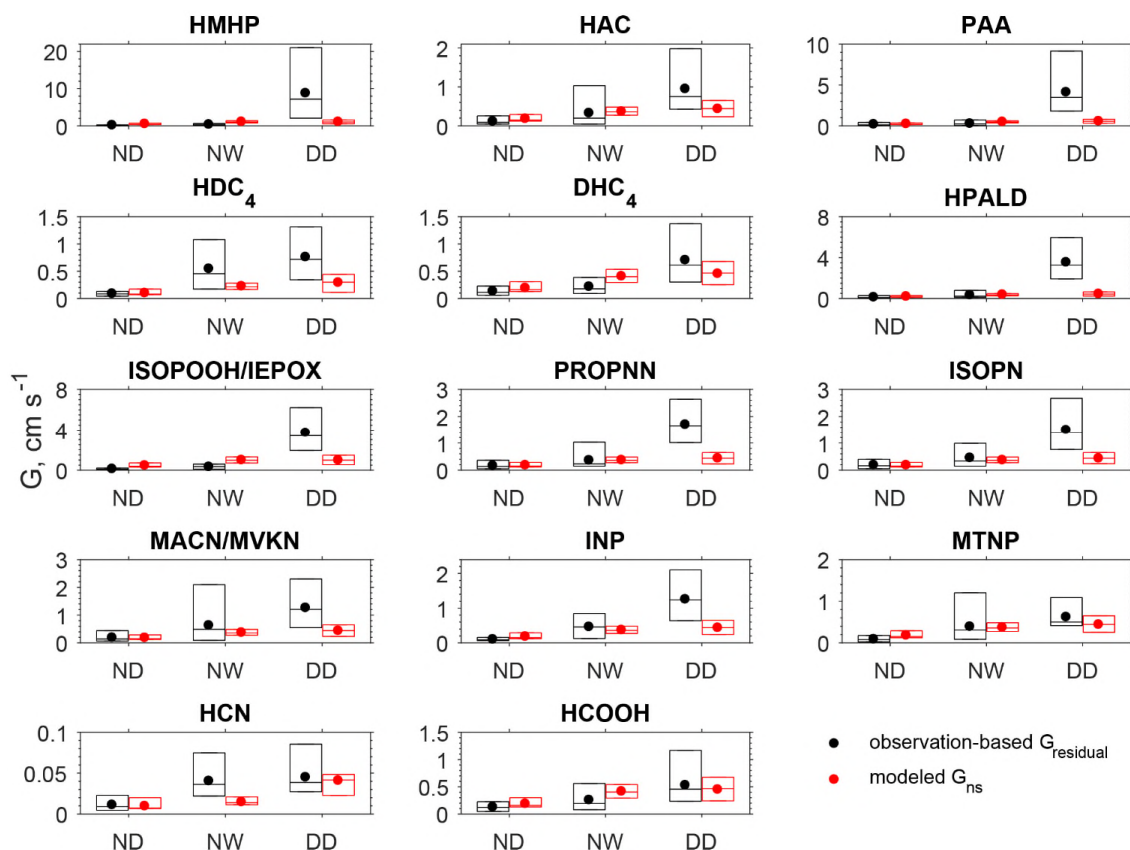


Figure 3. Box plot of the observation-based residual conductance ($G_{residual}$) and the modeled non-stomatal conductance (G_{ns}) during nighttime dry period (ND, $n=88$), nighttime wet period (NW, $n=40$), and daytime dry period (DD, $n=85$). In each box, the central mark is the median, and the edges of the box are the 25th and 75th percentiles. The filled dots represent the arithmetical mean of data between 25th and 75th percentiles. Daytime is 09:00-17:00 (local time) and nighttime is 20:00-06:00 (local time). The wet surface conditions were determined in the model driven by the observations of relative humidity, precipitation rate, friction velocity, and temperature.

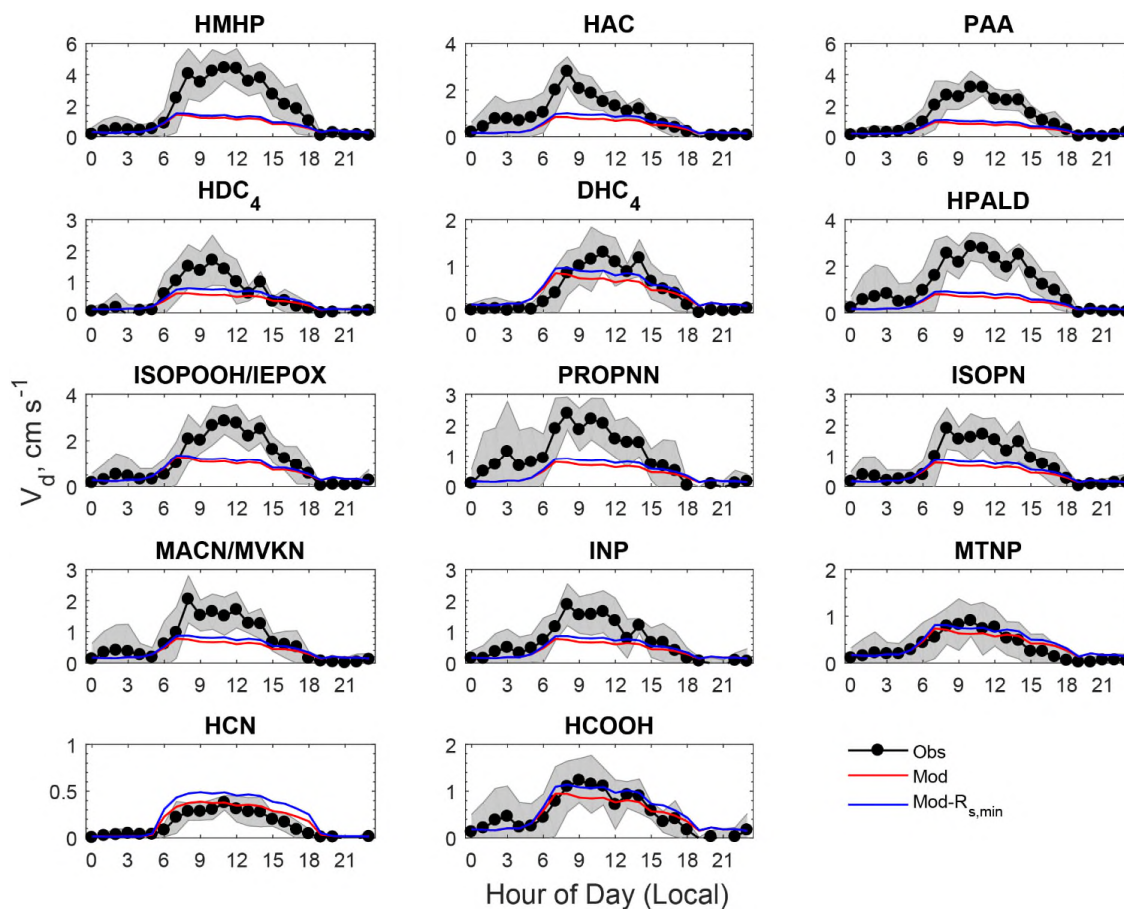


Figure 4. Comparison of averaged diel cycles of observed and modeled dry deposition velocities (V_d) of oVOCs and HCN. The shaded area indicates the standard deviation of the observations. “Mod- $R_{s,min}$ ” refers to a sensitivity test in which $R_{s,min}$ was reduced by 40%.

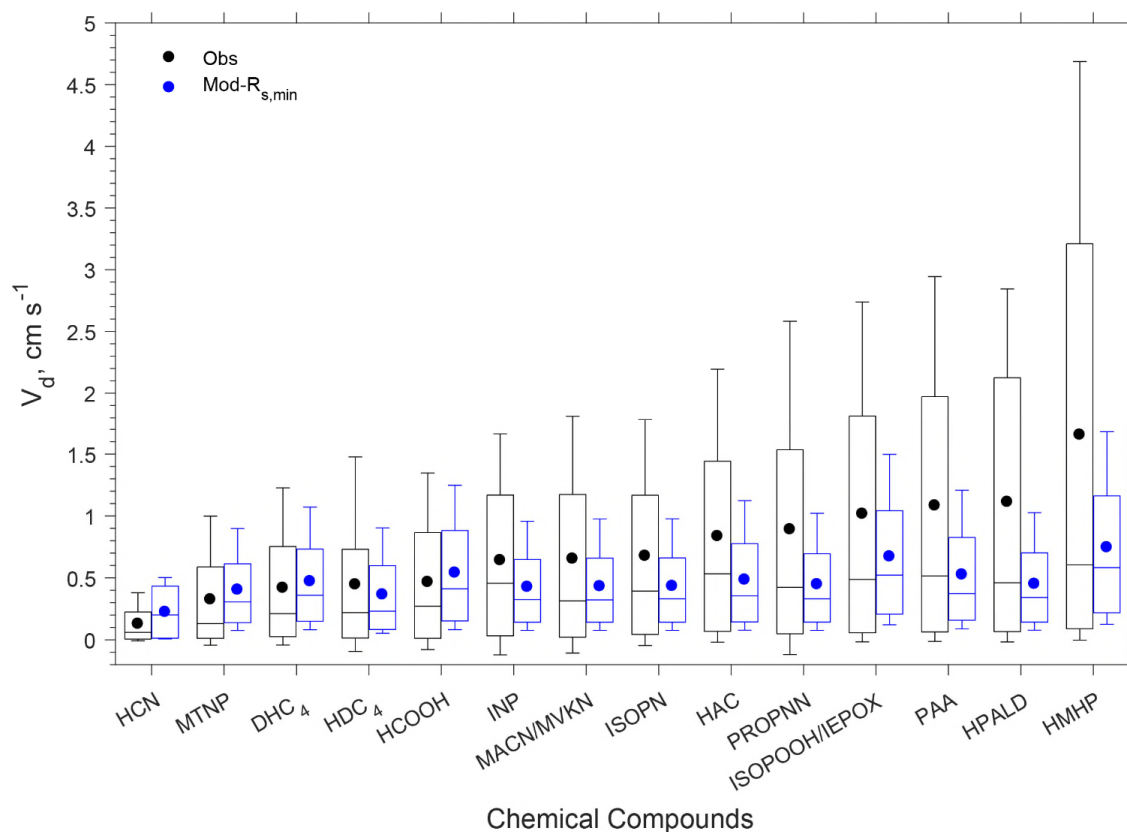


Figure 5. Box plot of observed and modeled hourly dry deposition velocities (V_d) of oVOCs and HCN. In each box, the central mark is the median, the edges of the box are the 25th and 75th percentiles, and the whiskers extend to the 10th and 90th percentiles. The filled dots represent the arithmetical mean of all the data. “Mod- $R_{s,min}$ ” refers to a sensitivity test in which $R_{s,min}$ was reduced by 40%.

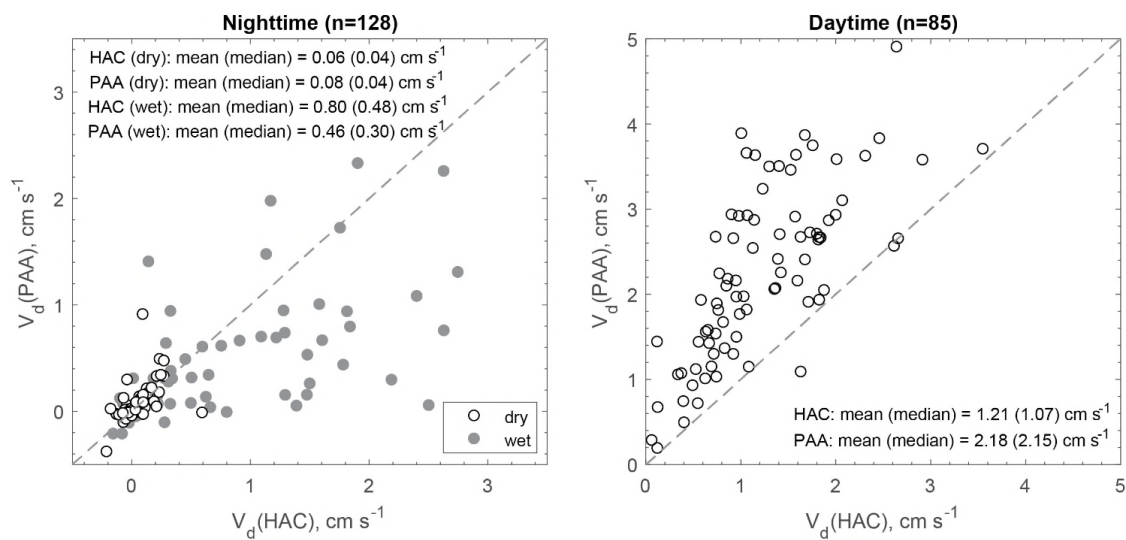


Figure 6. Scatter plot of the measured dry deposition velocities (V_d) for hydroxyacetone (HAC) and peroxyacetic acid (PAA) during nighttime (20:00-06:00, local time) and daytime (09:00-17:00, local time). The shaded (white) cycles correspond to the wet (dry) surface conditions.